Effects of interface states and temperature on the *C-V* behavior of metal/insulator/AlGaN/GaN heterostructure capacitors

Marcin Miczek,[1,2,a)] Chihoko Mizue,[1] Tamotsu Hashizume,[1,b)] and Bogusława Adamowicz[2]
[1]*Research Center for Integrated Quantum Electronics and Graduate School of Electronics and Information Engineering, Hokkaido University, North 13 West 8, 060-8628 Sapporo, Japan*
[2]*Institute of Physics, Silesian University of Technology, Krzywoustego 2, 44-100 Gliwice, Poland*

(Received 13 December 2007; accepted 10 March 2008; published online 28 May 2008)

The impact of states at the insulator/AlGaN interface on the capacitance-voltage (*C-V*) characteristics of a metal/insulator/AlGaN/GaN heterostructure (MISH) capacitor was examined using a numerical solver of a Poisson equation and taking into account the electron emission rate from the interface states. A parallel shift of the theoretical *C-V* curves, instead of the typical change in their slope, was found for a MISH device with a 25-nm-thick AlGaN layer when the SiN_x/AlGaN interface state density $D_{it}(E)$ was increased. We attribute this behavior to the position of the Fermi level at the SiN_x/AlGaN interface below the AlGaN valence band maximum when the gate bias is near the threshold voltage and to the insensitivity of the deep interface traps to the gate voltage due to a low emission rate. A typical stretch out of the theoretical *C-V* curve was obtained only for a MISH structure with a very thin AlGaN layer at 300 °C. We analyzed the experimental *C-V* characteristics from a SiN_x/Al_2O_3/AlGaN/GaN structure measured at room temperature and 300 °C, and extracted a part of $D_{it}(E)$. The relatively low D_{it} ($\sim 10^{11}$ eV^{-1} cm^{-2}) in the upper bandgap indicates that the SiN_x/Al_2O_3 bilayer is applicable as a gate insulator and as an AlGaN surface passivant in high-temperature, high-power AlGaN/GaN-based devices. © *2008 American Institute of Physics*. [DOI: 10.1063/1.2924334]

I. INTRODUCTION

GaN-based metal/insulator/semiconductor heterostructure field effect transistors (MISHFETs) have recently attracted much attention. While keeping the merits of conventional Schottky-gate-based HFETs, i.e., a high density of two-dimensional electron gas (2DEG) at the AlGaN/GaN interface, high cutoff and maximum frequencies, and the thermal and chemical stability of AlGaN and GaN, MISHFETs offer many advantages over HFETs, such as lower gate leakage current, higher breakdown voltage, better thermal stability of the gate, mitigation of current collapse, a wider range of gate voltage sweep, and higher maximum drain current and output power.[1–17] These features are crucial for applications in high-power, high-temperature electronics,[7,17] particularly to realize low on-resistance and normally off high-power FETs.[15,18]

Although the standard high frequency capacitance-voltage (*C-V*) measurement at room temperature (RT) is usually done on metal/insulator/semiconductor heterostructure (MISH) capacitors and/or metal/semiconductor heterostructure (MSH) Schottky diodes before the fabrication and characterization of the MISHFET devices, the *C-V* data are often used only to estimate the thicknesses of the insulator film and/or the AlGaN layer[1,4,12,16,19] or to calculate the 2DEG density.[1,20] Although some authors have claimed that the slope of the MISH *C-V* curve can be used as a measure of the electronic quality of the insulator/AlGaN interface,[4,11,13] this claim should be considered very carefully because the *C-V* slope in a metal/AlGaN/GaN structure depends on the quality of the AlGaN/GaN interface and other factors,[21] and there is no well known and tested procedure for the analysis of *C-V* curves from a metal/insulator/AlGaN/GaN structure to extract the state density at the insulator/AlGaN and AlGaN/GaN interfaces. Some other authors have stated that the shifts of the *C-V* curve and of the threshold voltage (V_{th}) with respect to theoretical values are related to the charge in the insulator and at the insulator/AlGaN interface.[6,7,12] The thermal stability of V_{th} has also been proposed as a criterion for high quality insulator/AlGaN interfaces.[10]

Surprisingly, little systematic experimental and theoretical study has been done on the high-temperature *C-V* behavior of MISH capacitors and MSH diodes considering the impact of the interface states. The *C-V* and deep level transient spectroscopy (DLTS) results of Mosca *et al.*[22] suggested that the influence of deep levels is crucial to gain an understanding of and improve the insulator/AlGaN interface. We stress, though, that *C-V* measurements done only at RT are far from sufficient to characterize wide bandgap GaN and AlGaN interfaces because of the extremely long time constants for electron emission from the deep states at RT (approximately 3 months for a level at 1 eV below the conduction band minimum in GaN) and an additional factor, such as higher temperature or light, is absolutely necessary to excite carriers from the deep levels.[2,22–24]

Therefore, in this work, we performed systematic calculations of theoretical *C-V* curves from $SiN_x/Al_{0.25}Ga_{0.75}N$/GaN structures with various thicknesses of SiN_x and the AlGaN layer, different densities, and distributions of the states at the SiN_x/AlGaN interface at RT, 300 °C, or 500 °C, taking into account the low rate of electron emission from the deep levels. A parallel shift of the

[a)]On leave from Institute of Physics, Silesian University of Technology, Gliwice, Poland. Electronic mail: marcin.miczek@polsl.pl.
[b)]Electronic mail: hashi@rciqe.hokudai.ac.jp.

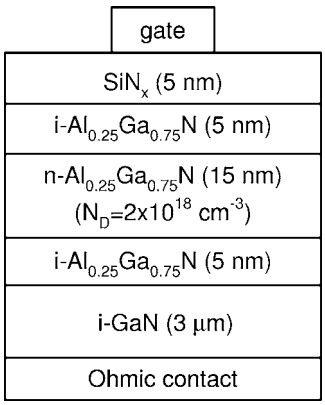

FIG. 1. Model structure used in the calculations.

theoretical *C-V* curves instead of the expected change in their slope was found in the studied devices with a 25-nm-thick AlGaN layer at RT and at 300 °C when the SiN_x/AlGaN interface state density $D_{it}(E)$ was increased. We attributed this behavior to the position of the Fermi level at the SiN_x/AlGaN interface below the valence band maximum of AlGaN when the gate bias was near the threshold voltage and to insensitivity of the deep interface traps to the gate voltage due to a low emission rate. The typical stretch out of the theoretical *C-V* curve was obtained in a structure with a thin (5 nm) AlGaN layer at 300 °C. We then compared the calculation results with experimental data from a SiN_x/Al_2O_3/AlGaN/GaN device and the Al_2O_3/AlGaN interface state density was determined for part of the AlGaN bandgap.

II. CALCULATION METHOD

A. Model structure and Poisson equation

To calculate a theoretical *C-V* curve from a metal/SiN_x/AlGaN/GaN structure, we solved a Poisson equation for the electric potential profile $V(x)$ using a one-dimensional model of the structure (Fig. 1). In AlGaN and GaN layers, the Poisson equation has the following form:

$$\frac{d^2V}{dx^2} = -\frac{q}{\varepsilon_S \varepsilon_0}(N_D - n + p), \tag{1}$$

where q is the elementary charge, ε_S is the dielectric constant of the semiconductor, ε_0 is vacuum permittivity, and N_D, n, and p are the concentrations of ionized donor dopants, electrons, and holes, respectively. In the insulator, Eq. (1) becomes the Laplace equation,

$$\frac{d^2V}{dx^2} = 0. \tag{2}$$

Boundary conditions at the contacts are the Dirichlet type, i.e., at the gate ($x=0$) $V = V_G - \phi_s/q + \phi_b/q$, where V_G is the gate voltage, ϕ_s and ϕ_b are the surface barrier height and a built-in potential (both in energy unit), respectively,[25] and $V=0$ at the Ohmic contact. At the interfaces (SiN_x/AlGaN and AlGaN/GaN), Neumann boundary conditions are imposed. For instance, at the insulator/AlGaN interface,

$$\varepsilon_S \varepsilon_0 F_S - \varepsilon_I \varepsilon_0 F_I = Q_{it} + Q_{fix}, \tag{3}$$

where ε_I is the insulator dielectric constant, $F = -dV/dx$ is the electric field intensity (subscripts S and I denote the semiconductor and the insulator, respectively), and Q_{it} and Q_{fix} are the sheet density of the interface trap charge and that of the interface fixed charge, respectively.

B. Interface state charge

As mentioned, because of the wide bandgap of GaN and AlGaN, the time constant of electron emission from the deep electronic states reaches very large values, particularly at RT. We can calculate the time constant for the trap level at energy E using the Shockley–Read–Hall model,[26]

$$\tau = \frac{1}{N_C v \sigma} \exp\left(\frac{E_C - E}{kT}\right), \tag{4}$$

where N_C, v, σ, E_C, k, and T are the effective density of states in the conduction band, the thermal velocity of electrons, the capture cross section of the trap, the bottom of the conduction band, the Boltzmann constant, and temperature, respectively.

Under the assumption that all interface states are in the thermal equilibrium with the semiconductor, the charge in the interface traps is determined by the Fermi–Dirac distribution $f(E)$,[27]

$$Q_{it} = q\int_{E_V}^{E_C} D_{it}^D(E)[1 - f(E)]dE - q\int_{E_V}^{E_C} D_{it}^A(E) f(E) dE, \tag{5}$$

where E_V is the top of the valence band and $D_{it}^D(E)$ and $D_{it}^A(E)$ are the energetic distribution of donorlike states and acceptorlike states, respectively. However, if the interface Fermi level (E_F) is lowered with respect to E_C by the negative gate voltage (V_G) within time (t), which is much smaller than the time constant (τ), only some of the electrons (determined by the emission efficiency) will be emitted from the interface traps. The emission efficiency is given by

$$\eta_e = 1 - \exp\left(-\frac{t}{\tau}\right). \tag{6}$$

Assuming that the interface states were in equilibrium at zero gate bias and the negative V_G was then applied, the charge in the interface traps should be expressed by

$$Q_{it} = q\int_{E_V}^{E_C} D_{it}^D(E)[1 - f_0(1 - \eta_e) - \eta_e f]dE - q\int_{E_V}^{E_C} D_{it}^A(E) \times [f_0(1 - \eta_e) + \eta_e f]dE, \tag{7}$$

where f_0 and f are the Fermi–Dirac function at zero bias and at the negative bias in question, respectively. It is easy to check that if $\eta_e = 1$, Eq. (7) is transformed to the classical formula [Eq. (5)]. We assumed here and in the further calculations that the measurement duration is of $t = 100$ s, which is a reasonable estimation for typical *C-V* measurements in the gate voltage range from 0 to −10 V with a sweeping rate of 100 mV/s. The values of the capture cross section of the interface states [σ in Eq. (4)] have not been reported for

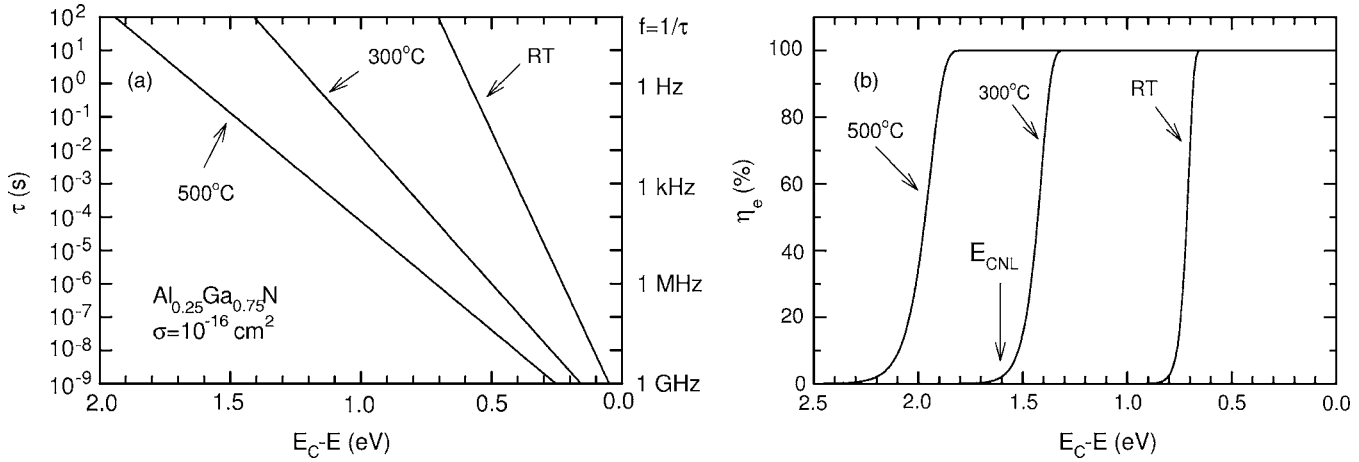

FIG. 2. (a) Time constant of electron emission from the interface traps to the $Al_{0.25}Ga_{0.75}N$ conduction band and (b) emission efficiency vs trap energy at RT, 300 °C, and 500 °C. Parameters for the calculation were taken from Table I.

insulator/AlGaN interfaces. Thus, we referred to the typical value of σ (10^{-16} cm^2) reported for SiO_2/Si interfaces.[28,29] The dependencies of τ and η_e versus the trap energy at RT, 300 °C, and 500 °C are plotted in Figs. 2(a) and 2(b), respectively. Note that $\eta_e(E)$ is a steplike function at RT and becomes more blurred at higher temperatures.

During the calculation, two types of the energetic distribution of electronic state density at the SiN_x/AlGaN interface, $D_{it}(E)$, were assumed. One type of $D_{it}(E)$ is a narrow Gaussian curve describing defect discrete states,

$$D_{it}^{A,D}(E) = D_{it\,max} \exp\left[-4 \log 2\left(\frac{E - E_{A,D}}{FWHM}\right)^2\right], \quad (8)$$

where $D_{it\,max}$ is the maximum density, $E_{A,D}$ is the energetic location of the level, and FWHM is the full width at half maximum of the Gaussian curve (subscripts A and D are used as previously). The donorlike discrete state at $E_D = E_C - 0.37$ eV, which is probably related to the N-vacancy defect,[30,31] and the acceptorlike state at $E_A = E_V + 1.0$ eV, which is related to the Ga vacancy,[32,33] were assumed [Fig. 3(a)]. FWHM of 0.1 eV was set for both states.

The other kind of $D_{it}(E)$ is a U-shaped distribution in accordance with the disorder-induced gap state model[34] with donorlike states below the charge neutrality level E_{CNL} and acceptorlike states above it. The density of the states reaches the minimum, denoted D_{it0}, at E_{CNL} [Fig. 3(b)], and the full formula for $D_{it}(E)$ is

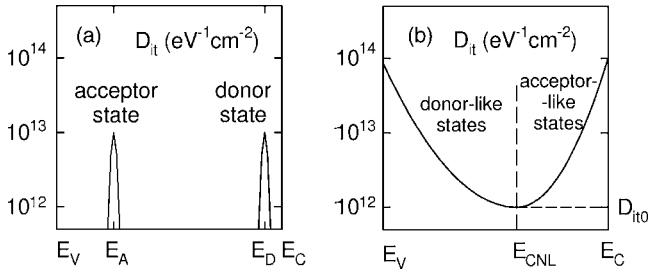

FIG. 3. SiN_x/AlGaN interface state density distribution used in the calculations: (a) the Gaussian peaks at $E_A = E_V + 1$ eV and at $E_D = E_C - 0.3$ eV and (b) the U-shaped distribution with E_{CNL} at 1.6 eV below E_C.

$$D_{it}^{A,D}(E) = D_{it0} \exp\left[\left(\frac{|E - E_{CNL}|}{E_{0A,0D}}\right)^{n_{A,D}}\right], \quad (9)$$

where E_{0A}, n_A, E_{0D}, and n_D describe the curvature of the acceptorlike branch (subscript A, $E_{CNL} < E < E_C$) and the donorlike one (subscript "D", $E_V < E < E_{CNL}$), respectively. Based on Ref. 35, we estimated E_{CNL} to be at $E_C - 1.1$ eV in GaN and at $E_C - 1.6$ eV in AlGaN.

C. Polarization charge

The piezoelectric polarization due to biaxial strain at the AlGaN/GaN interface is expressed by the following formula:[36]

$$P_{pe}(\text{AlGaN/GaN}) = P_{pe}(\text{AlGaN}) - P_{pe}(\text{GaN}) = 2\left(\frac{a_{GaN}}{a_{AlGaN}} - 1\right)\left(e_{31} - e_{33}\frac{C_{13}}{C_{33}}\right), \quad (10)$$

where a_{GaN} and a_{AlGaN} are the respective lattice constants of GaN and AlGaN, e_{31} and e_{33} are piezoelectric constants, and C_{13} and C_{33} are elastic constants. We can calculate the spontaneous polarization at the AlGaN/GaN interface from

$$P_{sp}(\text{AlGaN/GaN}) = P_{sp}(\text{AlGaN}) - P_{sp}(\text{GaN}), \quad (11)$$

where P_{sp}(AlGaN) and P_{sp}(GaN) are the spontaneous polarization in AlGaN and GaN, respectively.

Finally, the polarization-related fixed charge at the AlGaN/GaN interface is

$$Q_{fix}(\text{AlGaN/GaN}) = |P_{pe}(\text{AlGaN/GaN}) + P_{sp}(\text{AlGaN/GaN})|, \quad (12)$$

which gives about 1.2×10^{13} q/cm^2 at the $Al_{0.25}Ga_{0.75}N$/GaN interface. However, photoluminescence measurements by Grandjean *et al.*[37] and C-V measurements by Garrido *et al.*[38] provided actual values of the electric field intensity at AlGaN/GaN interfaces as low as 50% of the theoretical predictions. More recent electroreflectance results reported by Kurtz *et al.*[39] and Winzer *et al.*[40] showed smaller (~15%) discrepancies. Moreover, annealing during device processing can cause a partial relaxation of the interface

TABLE I. Parameters used in the calculations. m_e is the mass of a free electron, q is the elementary charge, and AlGaN denotes $Al_{0.25}Ga_{0.75}N$.

Parameter name	Symbol (unit)	Numerical value (material or interface)
Bandgap at RT	E_g (eV)	3.44 (GaN)[a]
		3.99 (AlGaN)[a]
		4.9 (SiN_x) [b]
Effective mass of electron	m_n/m_e	0.20 (GaN)[a]
		0.23 (AlGaN)[a]
Effective mass of hole	m_p/m_e	0.8 (GaN, AlGaN)[a]
Permittivity	ε	10.35 (GaN)[c]
		10.153 (AlGaN)[c]
		7.2 (SiN_x) [b]
Doping in the central AlGaN layer	(cm^{-3})	2×10^{18}
Background doping	(cm^{-3})	10^{14} (GaN)
		10^{15} (AlGaN)
Band offset	ΔE_C (eV)	0.384 (AlGaN/GaN)[d]
		0.8 (SiN_x/AlGaN) [b]
Surface barrier height	ϕ_s (eV)	2.0 (Al/SiN_x) [b]
Interface fixed charge	Q_{fix} (q/cm^2)	9×10^{12} (AlGaN/GaN)
Charge neutrality level	E_{CNL} (eV)	$E_C-1.6$ eV (SiN_x/AlGaN) [e]
		$E_C-1.1$ eV (AlGaN/GaN)[e]
Energy of donor discrete state	E_D (eV)	$E_C-0.37$ eV (SiN_x/AlGaN) [f]
Energy of acceptor discrete state	E_A (eV)	$E_V+1.0$ eV (SiN_x/AlGaN) [g]
FWHM of discrete states	FWHM (eV)	0.1
Capture cross section of interface states	σ (cm^2)	10^{-16} (SiN_x/AlGaN) [h]
Measurement duration	t (s)	100

[a]Reference 49.
[b]Reference 42.
[c]Reference 48.
[d]References 43 and 44.
[e]Reference 35.
[f]References 30 and 31.
[g]References 32 and 33.
[h]References 28 and 29.

strain and a decrease in the piezoelectric polarization.[41] Therefore, we adjusted Q_{fix} to 9×10^{12} q/cm^2 in our calculations to set the threshold voltage at a value comparable to that observed in our experiments.

We assumed no fixed charge at the SiN_x/AlGaN interface in accordance with the results of Maeda *et al.*[42] and the AlGaN/GaN interface was supposed to be free from bandgap states. Table I summarizes all parameters used in the computations. The parameter values for $Al_{0.25}Ga_{0.75}N$ were calculated from linear approximations using values for GaN and AlN, except the bandgap for which the bowing was taken into account. The supposed band offset at the AlGaN/GaN interface was 70% of the bandgap discontinuity.[43,44] The estimated influence of temperature on the band offset and the spontaneous and piezoelectric polarization at the $Al_{0.25}Ga_{0.75}N$/GaN interface[36,41,43,45–49] is negligible in the first approximation. Quantum corrections to the *C-V* curves are also unnecessary in the studied case.[50,51]

D. Numerical solution

The Poisson equation in the model structure was solved numerically by an elaborated computer program. First, the equation was linearized and transformed into a vector-matrix equation using the finite difference method, as proposed by Gummel,[52] for a nonuniform mesh and with appropriate boundary and interface conditions. During the computation of the electron density, the Fermi–Dirac integral was approximated analytically using the Aymerich-Humet formula.[53]

We supposed that the holes, as minority carriers, could follow neither the small ac voltage superposed on the gate bias nor the gate voltage sweep (the deep depletion mode); thus, the hole concentration was determined only at zero bias. The high frequency mode was used for the interface states, i.e., the states were assumed to not follow the ac signal, but to follow the gate voltage sweep with the restriction imposed by Eq. (7).

The vector-matrix equation was repeatedly solved for the correction in the electric potential until the correction was below $10^{-4}kT/q$. After the equation was solved for the gate voltage V_G and for $V_G+\Delta V_G$ ($\Delta V_G=0.01$ V), the differential capacitance C was computed.

III. CALCULATION RESULTS

A. General behavior and impact of temperature on the ideal *C-V* curve

Figure 4 clearly shows that our model reproduces the characteristic shape of *C-V* curves from the MISH capaci-

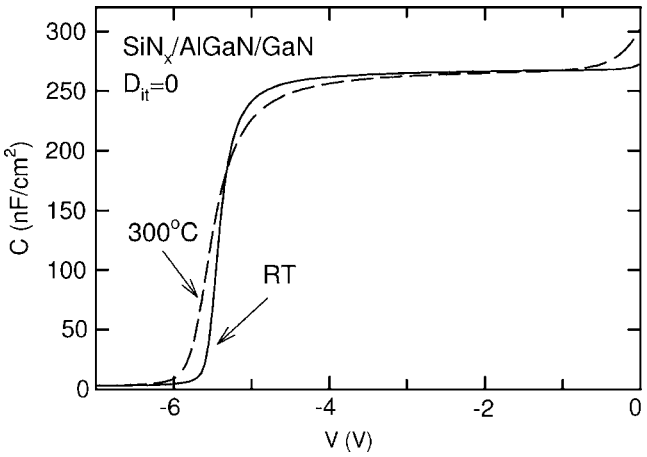

FIG. 4. Theoretical *C-V* curves calculated for a SiN_x/AlGaN/GaN structure like that in Fig. 1 without interface states at RT (solid line) and at 300 °C (dashed line).

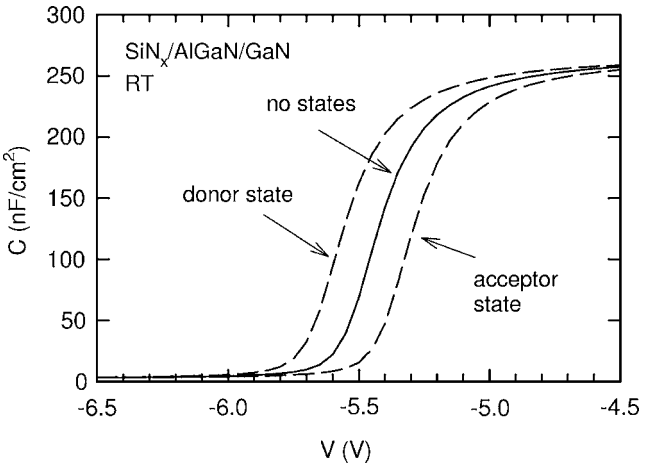

FIG. 5. *C-V* curves (dashed lines) calculated for a MISH diode like that in Fig. 1 at RT assuming acceptor- or donor-like states, respectively, at the SiN_x/AlGaN interface with density distributions like those of Fig. 3(a) and a maximum density of 10^{13} eV^{-1} cm^{-2}. The solid line represents the ideal *C-V* characteristics.

tors, namely, a nearly flat part between zero bias and the threshold voltage (V_{th}), a rapid change in the capacitance at V_{th}, and a very small capacitance in the subthreshold region (below V_{th}). The capacitance for the gate voltage between zero and V_{th} is determined by the total capacitance of the depleted AlGaN layer and SiN_x and is almost bias-independent. The capacitance in the subthreshold region depends on the background doping in the GaN layer and the small increase in the capacitance near zero bias is due to electron accumulation in the AlGaN layer.

The effect of increasing temperature on *C-V* from the MISH structure without interface states (Fig. 4) is similar to that in a MIS capacitor and manifests in a slight decrease of capacitance between V_{th} and zero and in a reduction of the slope caused by the increased Debye length and the thermal broadening of the Fermi–Dirac distribution.[27]

B. Effect of discrete interface traps

In this section, we discuss the influence of the discrete interface traps [with Gaussian density distribution, $D_{it}(E)$] on the *C-V* curve of the MISH structure with a 5-nm-thick SiN_x layer. As shown in Fig. 5, the discrete states (both the donor one at $E_C-0.3$ eV and the acceptor one at $E_V+1.0$ eV) act like a fixed charge at the SiN_x/AlGaN interface and only shift the *C-V* curve toward a more negative bias (the donor state) or toward zero (the acceptor state) with respect to the ideal characteristics. The shift is proportional to the density of states and does not depend on temperature up to at least 500 °C. Although such behavior is a little surprising compared to the well known *C-V* curve stretch out caused by the interface states in a MIS structure,[27,54] it can be explained since the relatively shallow donor state and the very deep acceptor state make it possible that the states are fully ionized throughout the studied gate bias range. This hypothesis was supported by calculations showing that if we assume an acceptor trap at $E_C-0.37$ eV or a donor trap at $E_V+1.0$ eV, the ideal *C-V* curve is not modified at all because the states are neutral in the studied bias range. The immunity of the shift to temperature can be explained using the concept of emission efficiency [$\eta_e(E)$] and Fig. 2(b). Namely, E_D is above the step of the $\eta_e(E)$ curve at RT and E_A is below the step of the curve even at 500 °C ($E_A=E_V+1.0$ eV$\approx E_C-3$ eV). Therefore, if the FWHM of the Gaussian $D_{it}(E)$ is not too large, the emission efficiency from

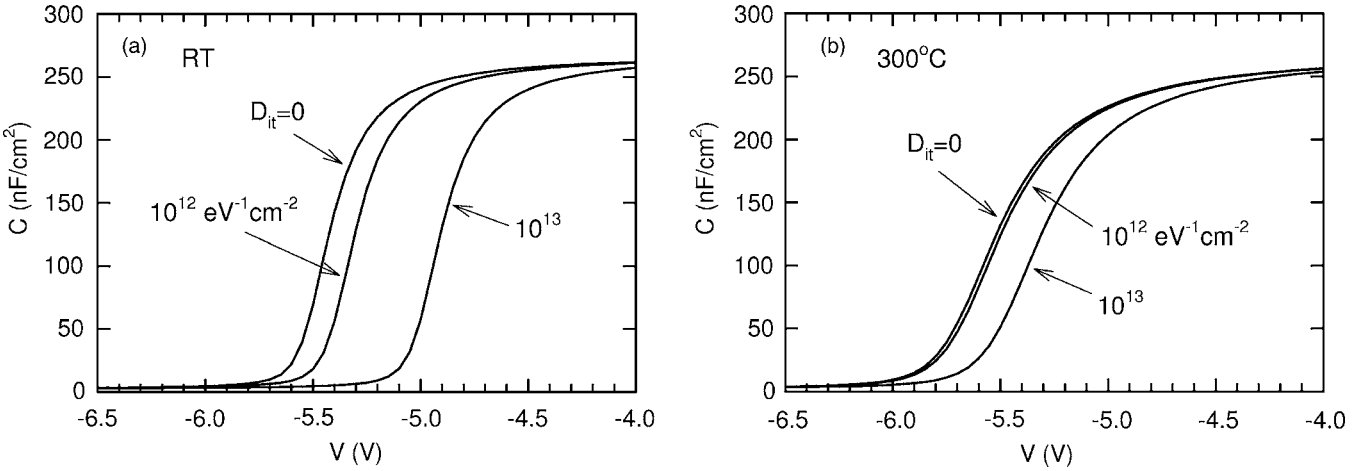

FIG. 6. Theoretical *C-V* curves calculated for the MISH capacitor with the SiN_x/AlGaN interface state density distribution, as shown in Fig. 3(b), and various interface state density minima D_{it0} (a) at RT and (b) at 300 °C.

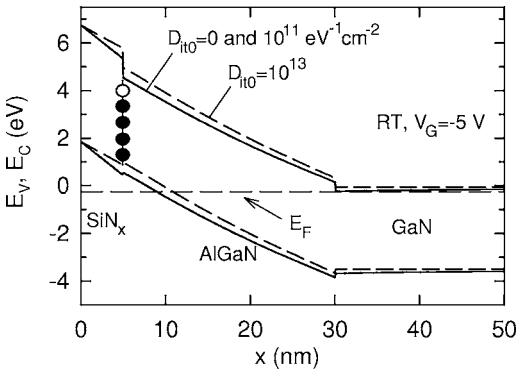

FIG. 7. Band diagrams of the SiN_x/AlGaN/GaN structure calculated at a bias of −5 V (slightly above the threshold) at RT. The SiN_x/AlGaN interface state density distribution was assumed to be like that of Fig. 3(b) with D_{it0}=0, 10^{11}, and 10^{13} eV^{-1} cm^{-2}.

the discrete states and, consequently, the *C-V* shift does not pronouncedly depend on temperature.

C. Effect of interface traps with a continuous distribution

Unexpectedly, the interface traps with the continuous *U*-shaped density distribution [Fig. 3(b)] also only shift the *C-V* curve without any change in its slope, as shown in Fig. 6. [The calculations were done for $D_{it0}=10^{12}$ and 10^{13} eV^{-1} cm^{-2}, although our and the others' experimental data indicates a lower value of D_{it0} (in the range of 10^{11} eV^{-1} cm^{-2}) in order to better demonstrate the effect of the interface states. For $D_{it0}=10^{11}$ eV^{-1} cm^{-2}, the shifts of *C-V* curves are much smaller and would not be well presented in the figures. The band diagrams for D_{it0} from 0 to 10^{13} eV^{-1} cm^{-2} and for $V_G=-5$ V are similar (Fig. 7) and the key point, i.e., the position of Fermi level below E_V at the SiN_x/AlGaN interface, holds for all cases.] In contrast to that of the discrete states, the shift depends on temperature, but the temperature influence is also peculiar in that increasing D_{it} has less impact on the *C-V* curve at higher temperatures [compare Figs. 6(a) and 6(b)].

To explain this *C-V* behavior, we calculated the band diagram of the structure at a bias slightly above V_{th} and the dependence of the charge in the SiN_x/AlGaN interface states (Q_{it}) versus gate voltage (V). As shown in Figs. 7 and 8, two reasons account for the limited sensitivity of Q_{it} to V.

(1) When V approaches V_{th} from zero bias, the Fermi level at the SiN_x/AlGaN interface (E_F) is already below the top of the AlGaN valence band E_V (Fig. 7), so the V-driven movement of E_F in the AlGaN bandgap cannot change the occupation of the interface states and Q_{it}. This is a fundamental limitation.
(2) When E_F is deeper and deeper in the AlGaN bandgap, the time constant of electron emission from the interface states close to E_F increases [Eq. (4) and Fig. 2(a)] and the emission efficiency decreases [Eq. (6) and Fig. 2(b)]; thus, Q_{it} becomes less and less sensitive to V [this can be seen when analyzing Eq. (7) for $\eta_e \rightarrow 0$]. Eventually, for a certain value of $V > V_{th}$, E_F is below the step of the $\eta_e(E)$ curve, and Q_{it} saturates and does not depend on V anymore, as demonstrated in Fig. 8(a). This limitation can be mitigated by increasing temperature.

The interface-state-related stretch out of the high frequency *C-V* curve[27,54] does not appear in the studied MISH structures because of the following:

(1) At RT, the zero-bias E_F at the SiN_x/AlGaN interface (E_{F0}) is below the step in the $\eta_e(E)$ curve and the interface charge is completely frozen. That is, the occupied states, both acceptor and donor ones, below E_{F0} cannot emit electrons because of the long time constant, even when E_F at the SiN_x/AlGaN interface is lowered with respect to E_C by the negative bias. The effect is demonstrated by the flat RT $Q_{it}(V)$ curve in Fig. 8(a) and schematically in Fig. 8(b).
(2) At higher temperatures, applying the negative bias causes the emission of electrons from the deeper acceptor states but only in the limited range of the gate voltage close to zero bias, as shown in Figs. 8(a) and 8(c). Unfortunately, in this range, the capacitance is almost

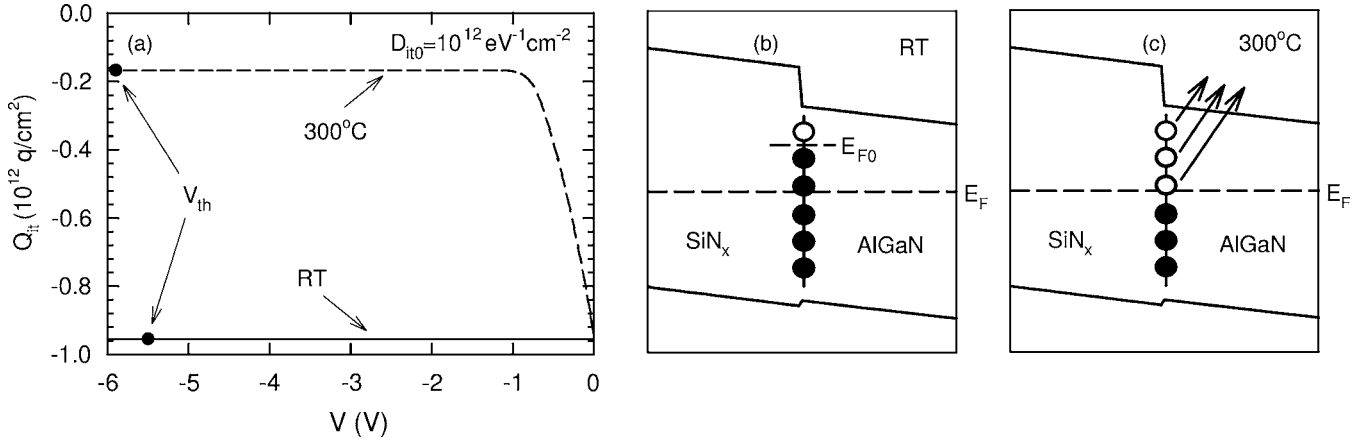

FIG. 8. (a) Dependence of the SiN_x/AlGaN interface state charge (Q_{it}) vs gate bias in the MISH diodes at RT (solid line) and at 300 °C (dashed line). The threshold voltages (V_{th}) are indicated for both curves. The interface state density distribution was assumed to be as shown in Fig. 3(b) with D_{it0} =10^{12} eV^{-1} cm^{-2}. (b) Schematic view of the SiN_x/AlGaN interface at RT for a gate bias slightly below zero and without electron emission from the interface states beneath the zero gate bias Fermi level (E_{F0}). The filled circles represent occupied states, and the empty circle the unoccupied state. (c) A similar view at 300 °C. The arrows indicate the electron emission from the interface states to the AlGaN conduction band.

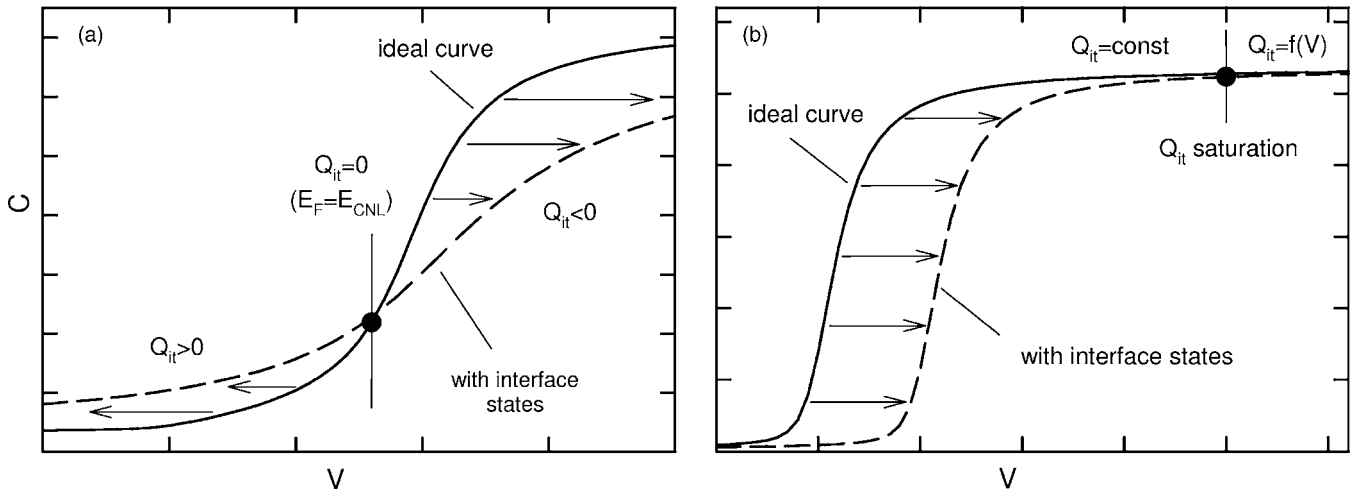

FIG. 9. Schematic illustration of (a) a typical interface-state-related stretch out of a high frequency *C-V* curve (e.g., for a SiO_2/Si MIS structure) and (b) peculiar fixed-charge-like behavior (e.g., in the studied MISH capacitor). Solid lines represent the ideal curves and the dashed lines represent those with interface states.

voltage-independent and although Q_{it} is sensitive to V, the flat *C-V* curve cannot be stretched out (the slope is equal to zero so it cannot be lowered by the interface states) or, in other words, the stretch out is degenerated into a parallel shift of the *C-V* curve (Fig. 9). Moreover, the change in Q_{it} is much lower than the 2DEG density, so the deformation of the *C-V* curve near a zero bias is small.

The described phenomena are of great importance in *C-V* analysis of metal/ /insulator/AlGaN/GaN devices because even if the *C-V* slope is close to the theoretical one for the ideal structure, the interface states can have quite a high density and be indistinguishable from a fixed charge. Moreover, if the intrinsic value of V_{th} (the value for the insulator/AlGaN interface without interface states and fixed charge) is not known, only the interface states lying between E_{F0} and the step in the $\eta_e(E)$ dependence at the maximal measurement temperature can be analyzed by the *C-V* technique. [It seems to be possible to shift the upper limit of $D_{it}(E)$ scanning above E_{F0} by using a positive gate voltage, but this can cause an uncontrolled shift of the *C-V* curves, probably due to charge trapping.[22]] The other states are inactive or act like a fixed charge. Therefore, evaluation of the insulator/AlGaN interface quality based only on RT *C-V* measurements of the MISH structure is inadequate because deeper states, which are frozen at RT, can manifest themselves at higher temperatures.

As can be deduced from the above analysis, the shift of V_{th} in respect to its intrinsic position, ΔV_{th}, depends on the value of Q_{it} when V reaches V_{th} and on the geometrical capacitance of the insulator/AlGaN system ($C_{I/AlGaN}$), i.e.,

$$\Delta V_{th} = -\frac{Q_{it}(V_{th})}{C_{I/AlGaN}}, \tag{13}$$

which is in agreement with the suggestion that ΔV_{th} is related to the charge at the insulator/AlGaN interface.[6,7,12]

Nevertheless, $Q_{it}(V_{th})$ and thus ΔV_{th} are complex functions of D_{it} and temperature in the case of continuous $D_{it}(E)$. As shown in Fig. 6(a), ΔV_{th} is positive in the studied structure and reaches about 0.6 V for $D_{it0}=10^{13}$ eV^{-1} cm^{-2} at RT. Surprisingly, ΔV_{th} is reduced to about 0.25 V at 300 °C for the same value of D_{it0} [Fig. 6(b)]. This effect is caused by the fact that the step of $\eta_e(E)$ is closer to E_{CNL} at 300 °C than that at RT [Fig. 2(b)] and $D_{it}(E)$ decreases while E approaches E_{CNL}, so the saturated Q_{it} is smaller. Other calculations (not shown) suggest that the magnitude and even the sign of ΔV_{th} depend on the SiN_x thickness, $D_{it}(E)$, and the position of E_{CNL}. [Note that if the step in the $\eta_e(E)$ curve is at E_{CNL}, ΔV_{th} should be close to zero even if $D_{it}(E)$ is large.] Since the value of E_{CNL} is not well known for AlGaN, quantitative analysis of *C-V* experimental data is very difficult.

On the other hand, the more important, from the practical point of view, temperature-induced shift of the *C-V* curve (with a slight decrease in the slope as described in Sec. III A) when $D_{it}(E)$ is fixed is systematic, as shown in Fig. 10. The thermal shift is negative and its absolute value is larger if D_{it} is higher. This is the direct consequence of the thermal movement of the step in $\eta_e(E)$ toward E_V [Fig. 2(b)], which enables deeper states to emit electrons so the value of Q_{it} is more positive at the threshold. Hence, our analysis confirms that the thermal stability of V_{th} can also be used as a criterion for high quality insulator/AlGaN interfaces.[10]

D. Stretch out of the *C-V* curve in the structure with a thin AlGaN layer

Analysis of the reasons for the peculiarity in the *C-V* characteristics of the MISH structure suggests that it should be possible to obtain the typical behavior by

(1) setting E_F at the SiN_x/AlGaN interface above E_V when the gate bias approaches the threshold voltage and
(2) widening the energy range of the interface states effectively emitting electrons.

The first can be achieved by thinning the AlGaN layer and the second by increasing temperature. Therefore, we did computations for a SiN_x(5 nm)/AlGaN(5 nm)/GaN struc-

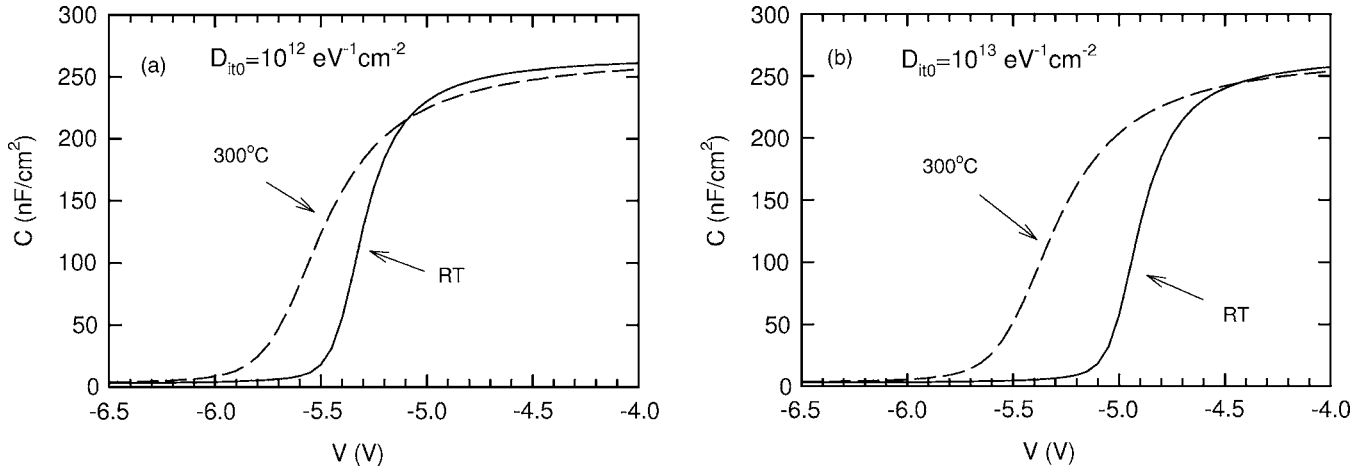

FIG. 10. Theoretical *C-V* curves calculated at RT and 300 °C for the MISH structure with the interface state density distribution shown in Fig. 3(b) and for D_{it0} fixed at (a) 10^{12} and (b) 10^{13} eV^{-1} cm^{-2}.

ture [Fig. 11(a)] with a SiN_x/AlGaN interface state density distribution like that in Fig. 3(b) with $D_{it0}=5\times10^{12}$ eV^{-1} cm^{-2} at 300 °C. It is evident from Fig. 11(b) that the classical stretch out of the *C-V* curve appears in this case. The band diagram [Fig. 12(a)] demonstrates that E_F at the SiN_x/AlGaN interface is above E_V when $V\approx V_{th}$ and Fig. 12(b) shows that Q_{it} is sensitive to V near V_{th}. However, E_F is quite far from E_C, so the *C-V* behavior at RT is still peculiar. The calculations indicate that the AlGaN thickness is a more critical factor than that of SiN_x regarding whether the stretch out is observed, e.g., it is present in SiN_x(10 nm)/AlGaN(5 nm)/GaN but not in SiN_x(5 nm)/AlGaN(10 nm)/GaN. This result is important for devices with an insulated recessed gate, which is promising for the fabrication of normally off MISHFETs.[18]

IV. COMPARISON TO EXPERIMENTAL RESULTS

A. Device fabrication

To test the theoretical model experimentally, we had MISH devices fabricated on an $Al_{0.25}Ga_{0.75}N$/GaN/sapphire wafer with a 25 nm modulation doped AlGaN layer provided by Matsushita Electric Industrial Co. Ltd. [Fig. 13(a)]. Before processing, the sample was chemically cleaned in acetone, ethanol, and water, and then the native oxide was removed in a HF:H_2O (1:5) solution. Next, the sample was exposed to nitrogen radicals in a molecular beam epitaxy (MBE) deposition chamber (the sample was kept at 300 °C, the processing time was 10 min, and the radio frequency source power was 350 W). A 1 nm Al layer was then deposited on the sample, which was kept at RT, and the Al/AlGaN/GaN system was annealed at 700 °C for 10 min in the MBE chamber. This process produces a thin Al_2O_3 layer and improves electronic and chemical properties of the AlGaN surface by reducing the amount of defects related to nitrogen vacancies and oxygen.[55] After this, the SiN_x film was deposited by the electron cyclotron resonance chemical vapor deposition (ECR CVD) technique (the sample was at 260 °C, the power was 100 W, and the deposition rate was about 10 nm/min) using SiH_4 and N_2 with a flow rate of 10 SCCM (SCCM denotes cubic centimeter per minute at STP), proceeded by 1 min of ECR CVD N_2 plasma treatment in the same chamber (the power was 50 W and the flow rate was 10 SCCM). We checked the thickness of the SiN_x layer by ellipsometric measurements of Si control samples mounted close to the AlGaN/GaN one and confirmed that it was approximately equal to 20 nm. Ohmic Ti/Al/Ti/Au contacts were formed by photolithography, wet etching in a buffered HF solution, metal layer deposition, lift-off, and rapid thermal annealing in nitrogen at 800 °C for 1 min. Finally, circular Al/Au gate contacts with diameters from 200 to 500 μm were formed.

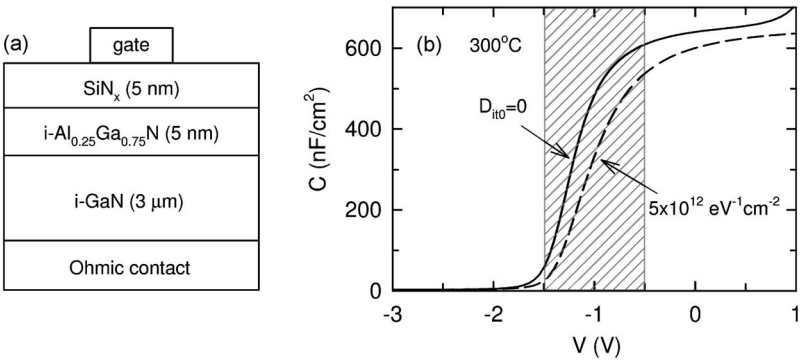

FIG. 11. (a) Another model structure used in the calculations. (b) Theoretical *C-V* curves for MISH structures like that in Fig. 11(a) without interface states (solid line) and with a SiN_x/AlGaN interface state density distribution like that in Fig. 3(b) with $D_{it0}=5\times10^{12}$ eV^{-1} cm^{-2} (dashed line) at 300 °C. The region of capacitance sensitivity to gate bias is marked.

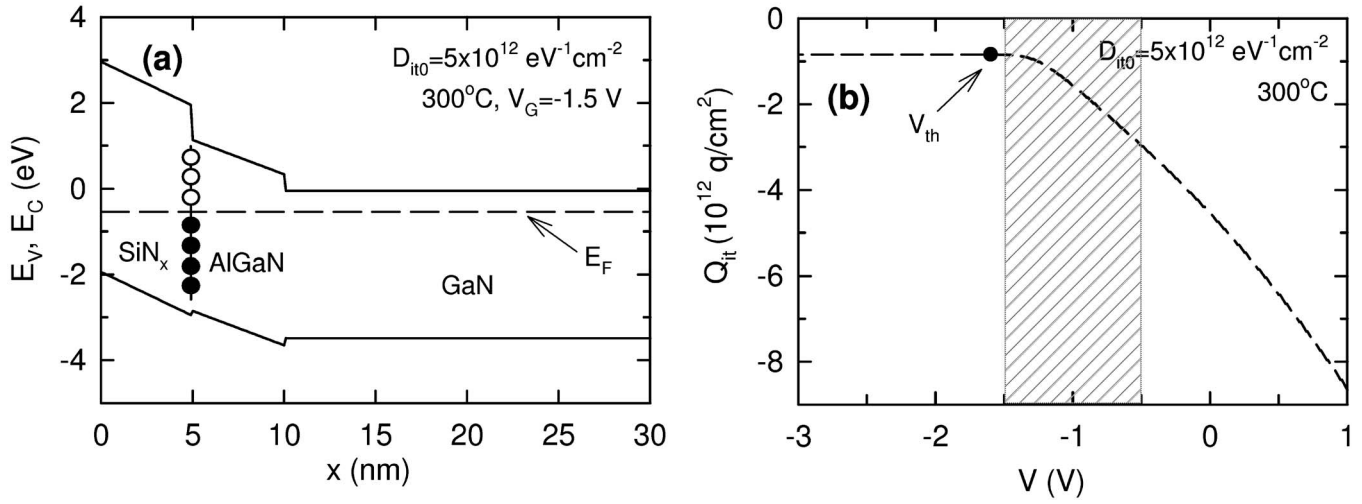

FIG. 12. (a) Band diagram of a MISH capacitor like that in Fig. 11(a) calculated at a bias slightly above the threshold voltage at 300 °C. The SiN_x/AlGaN interface state density distribution was assumed to be like that in Fig. 3(b) with $D_{it0}=5\times10^{12}$ eV^{-1} cm^{-2}. (b) Dependence of the SiN_x/AlGaN interface state charge (Q_{it}) vs gate bias related to the dashed *C-V* curve from Fig. 11(b). The region of capacitance sensitivity to gate bias is marked as in Fig. 11(b) and the threshold voltage (V_{th}) is indicated.

B. Measurements and fitting to experimental data

We characterized the fabricated $SiN_x/Al_2O_3/AlGaN/GaN$ devices by *C-V* measurements done at 100 kHz with an HP 4192A LF impedance analyzer. During the experiment, we kept the sample at RT or 300 °C in an evacuated chamber with an MMR K-20 programable temperature controller. The temperature was changed at a maximum rate of 10 °C/min. No thermal degradation of the devices was observed after the high-temperature *C-V* measurements. To estimate the effects that the fixed charge in SiN_x and the gate metal barrier height had on the *C-V* curves, we measured and analyzed a SiN_x/Si MIS structure.

The experimental *C-V* characteristics for a voltage sweep from 0 to −15 V are shown in Fig. 13(b) (circles and squares) together with fitted theoretical curves (lines). The hysteresis loop widths were 0.15 and 0.5 V at RT and 300 °C, respectively. To adjust the *C-V* slope in the threshold region, we assumed the *U*-shaped $D_{it}(E)$ at the AlGaN/GaN interface with $D_{it0}=10^{11}$ eV^{-1} cm^{-2} and with a shape similar to that in Fig. 3(b). The background doping in GaN and the fixed charge at the AlGaN/GaN interface were fitted to be 4×10^{14} cm^{-3} and 8.5×10^{12} q/cm^2, respectively. The capacitance between zero gate bias and V_{th} is in good agreement with the geometrical capacitance of a SiN_x(20 nm)/Al_2O_3(1 nm)/AlGaN(25 nm) system.

To fit the thermal shift of *C-V* curves, the continuous $D_{it}(E)$ was assumed at the Al_2O_3/AlGaN interface as in Fig. 13(c). Good fitting [Fig. 13(b)] was obtained for $D_{it0}=10^{11}$ eV^{-1} cm^{-2}. The deviation of the theoretical line from the experimental data at RT for the gate voltage between −11 and −10.3 V can be caused by a non-*U*-shaped $D_{it}(E)$ or some bulk levels in the actual MISH structure. The low value of D_{it0} should be interpreted carefully taking into account that the thermal *C-V* shift is related only to the interface

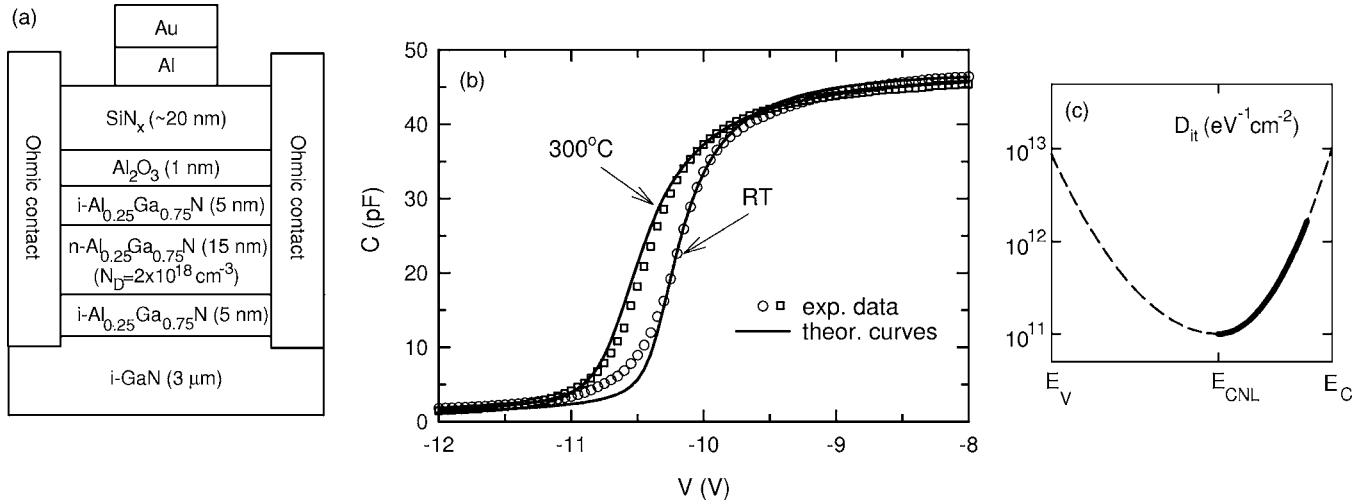

FIG. 13. (a) Schematic diagram of the fabricated $SiN_x/Al_2O_3/AlGaN/GaN$ structure. (b) Experimental *C-V* characteristics from the MISH capacitor measured at RT (circles) and 300 °C (squares) and fitted theoretical curves (lines). (c) $D_{it}(E)$ assumed in the calculation of the best fitted curve. The part of $D_{it}(E)$ actually determined from the fitting is shown by the bold solid line.

states between E_{F0} at RT and the step in the $\eta_e(E)$ curve at 300 °C [Fig. 2(b)], i.e., $E_C-0.25$ eV and $E_C-1.6$ eV, respectively [the bold part of the $D_{it}(E)$ curve in Fig. 13(c)]. Thus, the density of the interface states outside of this energetic interval was not determined. Nevertheless, the good thermal stability indicates the high electronic and chemical quality of $SiN_x/Al_2O_3/AlGaN$ system.

V. CONCLUSION

We performed systematic calculations and analysis of theoretical *C-V* curves from $SiN_x/Al_{0.25}Ga_{0.75}N/GaN$ structures with various SiN_x and AlGaN layer thicknesses, different densities, and distributions of states at the $SiN_x/AlGaN$ interface, $D_{it}(E)$, at RT, 300 °C, and 500 °C, taking into account the low rate of electron emission from deep interface traps. We found and explained an unusual influence of the electronic states at the $SiN_x/AlGaN$ interface on *C-V* curves at RT and 300 °C, i.e., a shift instead of a stretch out. The interface-state-related shift of the threshold voltage V_{th} is a complicated function of the magnitude and the shape of the energetic distribution of the state density and temperature. On the other hand, the thermal shift of V_{th} when $D_{it}(E)$ is fixed is systematic and at least semiquantitative analysis of experimental *C-V* data is possible, although the studied energetic interval of $D_{it}(E)$ is limited. After the analysis of the *C-V* peculiarity, we obtained the typical *C-V* curve stretch out in a structure with a 5-nm-thick AlGaN layer at 300 °C.

We compared the calculation results to experimental data from a $SiN_x/Al_2O_3/AlGaN/GaN$ device. The good thermal stability of the MISH capacitor indicated a low density of states (10^{11} eV^{-1} cm^{-2} at the minimum) at the $Al_2O_3/AlGaN$ interface and showed that a SiN_x/Al_2O_3 bilayer is promising for use as a gate insulator and as a passivating film for AlGaN/GaN-based MISH devices applied in high-temperature, high-power electronics.

ACKNOWLEDGMENTS

One of the authors (M.M.) thanks RCIQE, Hokkaido University, Sapporo, Japan for the postdoctoral fellowship and all members of RCIQE for their kind help. The work was partially supported within Project No. 1561/T11/2005/29 by the Polish Ministry of Science and Higher Education.

[1] M. A. Khan, X. Hu, G. Sumin, A. Lunev, J. Yang, R. Gaska, and M. S. Shur, IEEE Electron Device Lett. **21**, 63 (2000).
[2] M. A. Khan, X. Hu, A. Tarakji, G. Simin, J. Yang, R. Gaska, and M. S. Shur, Appl. Phys. Lett. **77**, 1339 (2000).
[3] A. Tarakji, X. Hu, A. Koudymov, G. Simin, J. Yang, M. A. Khan, M. S. Shur, and R. Gaska, Solid-State Electron. **46**, 1211 (2002).
[4] K.-Y. Park, H.-I. Cho, J.-H. Lee, S.-B. Bae, C.-M. Jeon, J.-L. Lee, D.-Y. Kim, C.-S. Lee, and J.-H. Lee, Phys. Status Solidi C **0**, 2351 (2003).
[5] W. S. Tan, P. A. Houston, G. Hill, R. J. Airey, and P. J. Parbook, J. Electron. Mater. **32**, 350 (2003).
[6] V. Adivarahan, M. Gaevski, W. H. Sun, H. Fatima, A. Koudymov, S. Saygi, G. Simin, J. Yang, M. A. Khan, A. Tarakji, M. S. Shur, and R. Gaska, IEEE Electron Device Lett. **24**, 541 (2003).
[7] M. A. Khan, G. Simin, J. Yang, J. Zhang, A. Koudymov, M. S. Shur, R. Gaska, X. Hu, and A. Tarakji, IEEE Trans. Microwave Theory Tech. **51**, 624 (2003).
[8] K.-Y. Park, H.-I. Cho, H.-C. Choi, Y.-H. Bae, C.-S. Lee, J.-L. Lee, and J.-H. Lee, Jpn. J. Appl. Phys., Part 2 **43**, L1433 (2004).
[9] C. K. Wang, R. W. Chuanga, S. J. Changa, Y. K. Sua, S. C. Wei, T. K. Lin, T. K. Ko, Y. Z. Chiou, and J. J. Tang, Mater. Sci. Eng., B **119**, 25 (2005).
[10] C. Wang, N. Maeda, M. Hiroki, T. Kobayashi, and T. Enoki, Jpn. J. Appl. Phys., Part 1 **44**, 7889 (2005).
[11] P. D. Ye, B. Yang, K. K. Ng, J. Bude, G. D. Wilk, S. Halder, and J. C. M. Hwang, Appl. Phys. Lett. **86**, 063501 (2005).
[12] S. Arulkumaran, T. Egawa, and H. Ishikawa, Jpn. J. Appl. Phys., Part 2 **44**, L812 (2005).
[13] C. Liu, E. F. Chor, and L. S. Tan, Appl. Phys. Lett. **88**, 173504 (2006).
[14] M. Marso, G. Heidelberger, K. M. Indlekofer, J. Bernát, A. Fox, P. Kordoš, and H. Lüth, IEEE Trans. Electron Devices **53**, 1517 (2006).
[15] R. Wang, Y. Cai, C.-W. Tang, K. May Lau, and K. J. Chen, IEEE Electron Device Lett. **27**, 793 (2006).
[16] P. Kordoš, D. Gregušová, R. Stoklas, K. Čičo, and J. Novák, Appl. Phys. Lett. **90**, 123513 (2007).
[17] H. Okumura, Jpn. J. Appl. Phys., Part 1 **45**, 7565 (2006).
[18] W. Saito, Y. Takada, M. Kuraguchi, K. Tsuda, and I. Omura, IEEE Trans. Electron Devices **53**, 356 (2006).
[19] J. Bernát, D. Gregušová, G. Heidelberger, A. Fox, M. Marso, H. Lüth, and P. Kordoš, Electron. Lett. **41**, 667 (2005).
[20] W. Wang, J. Derluyn, M. Germain, M. Leys, S. Degroote, D. Schreurs, and G. Borghs, Jpn. J. Appl. Phys., Part 2 **45**, L224 (2006).
[21] M. J. Uren, D. Lee, B. T. Hughes, P. J. M. Parmiter, J. C. Birbeck, R. Balmer, T. Martin, R. H. Wallis, and S. K. Jones, J. Cryst. Growth **230**, 579 (2001).
[22] R. Mosca, E. Gombia, A. Passaseo, V. Tasco, M. Peroni, and P. Romanini, Superlattices Microstruct. **36**, 425 (2004).
[23] J. A. Cooper, Jr., Phys. Status Solidi A **162**, 305 (1997).
[24] T. Hashizume, E. Alekseev, D. Pavlidis, K. S. Boutros, and J. Redwing, J. Appl. Phys. **88**, 1983 (2000).
[25] S. Selberherr, *Analysis and Simulation of Semiconductor Devices* (Springer, Wien, 1984).
[26] W. Shockley and W. T. Read, Phys. Rev. **87**, 835 (1952); R. N. Hall, *ibid.* **87**, 387 (1952).
[27] E. H. Nicollian and J. R. Brews, *MOS (Metal Oxide Semiconductor), Physics and Technology* (Wiley, New York, 1982).
[28] H. Deuling, E. Klausmann, and A. Goetzberger, Solid-State Electron. **15**, 559 (1972).
[29] K. Yamasaki, M. Yoshida, and T. Sugano, Jpn. J. Appl. Phys. **18**, 113 (1979).
[30] E. Yamaguchi and M. R. Junnarkar, J. Cryst. Growth **189–190**, 570 (1998).
[31] J. Kotani, S. Kasai, T. Hashizume, and H. Hasegawa, J. Vac. Sci. Technol. B **23**, 1799 (2005).
[32] J. Neugebauer and C. G. Van de Walle, Appl. Phys. Lett. **69**, 503 (1996).
[33] U. Kaufmann, M. Kunzer, H. Obloh, M. Maier, Ch. Manz, A. Ramakrishnan, and B. Santic, Phys. Rev. B **59**, 5561 (1999).
[34] H. Hasegawa and H. Ohno, J. Vac. Sci. Technol. B **4**, 1130 (1986).
[35] W. Mönch, Appl. Surf. Sci. **117–118**, 380 (1997); J. Robertson and B. Falabretti, J. Appl. Phys. **100**, 014111 (2006).
[36] O. Ambacher, M. Eickhoff, A. Link, M. Hermann, M. Stutzmann, F. Bernardini, V. Fiorentini, Y. Smorchkova, J. Speck, U. Mishra, W. Schaff, V. Tilak, and L. F. Eastman, Phys. Status Solidi C **0**, 1878 (2003).
[37] N. Grandjean, J. Massies, M. Leroux, M. Laügt, P. Lefebvre, B. Gil, J. Allègre, and P. Bigenwald, MRS Internet J. Nitride Semicond. Res. **4S1**, G11.7 (1999).
[38] J. A. Garrido, A. Jiménez, J. L. Sánchez-Rojas, E. Muñoz, F. Omnès, and P. Gibart, Phys. Status Solidi A **176**, 195 (1999).
[39] S. R. Kurtz, A. A. Allerman, D. D. Koleske, A. G. Baca, and R. D. Briggs, J. Appl. Phys. **95**, 1888 (2004).
[40] A. T. Winzer, R. Goldhahn, G. Gobsch, A. Link, M. Eickhoff, U. Rossow, and A. Hangleiter, Appl. Phys. Lett. **86**, 181912 (2005).
[41] D. Chen, B. Shen, K. Zhang, Y. Tao, X. Wu, J. Xu, R. Zhang, and Y. Zheng, Jpn. J. Appl. Phys., Part 1 **45**, 18 (2006).
[42] N. Maeda, M. Hiroki, N. Watanabe, Y. Oda, H. Yokoyama, T. Yagi, T. Makimoto, T. Enoki, and T. Kobayashi, Jpn. J. Appl. Phys., Part 1 **46**, 547 (2007).
[43] O. Ambacher, B. Foutz, J. Smart, J. R. Shealy, N. G. Weimann, K. Chu, M. Murphy, A. J. Sierakowski, W. J. Schaff, L. F. Eastman, R. Dimitrov, A. Mitchell, and M. Stutzmann, J. Appl. Phys. **87**, 334 (2000).
[44] G. Martin, S. Strite, A. Botchkarev, A. Agarwai, A. Rockettt, H. Morkoç,

W. R. L. Lambrecht, and B. Segall, Appl. Phys. Lett. **65**, 610 (1994); G. Martin, A. Botchkarev, A. Rockett, and H. Morkoç, *ibid.* **68**, 2541 (1996).
[45]V. Fuflyigin, E. Salley, A. Osinsky, and P. Norris, Appl. Phys. Lett. **77**, 3075 (2000).
[46]H. Iwanaga, A. Kunishige, and S. Takeuchi, J. Mater. Sci. **35**, 2451 (2000).
[47]R. R. Reeber and K. Wang, MRS Internet J. Nitride Semicond. Res. **6**, 3 (2001).
[48]J.-M. Wagner and F. Bechstedt, Phys. Rev. B **66**, 115202 (2002).
[49]I. Vurgaftman and J. R. Meyer, J. Appl. Phys. **94**, 3675 (2003).
[50]J. Yoshida, IEEE Trans. Electron Devices **33**, 154 (1986).
[51]R. Anholt, Solid-State Electron. **45**, 1189 (2001).
[52]H. K. Gummel, IEEE Trans. Electron Devices **11**, 455 (1964).
[53]X. Aymerich-Humet, F. Serra-Mestres, and J. Millán, Solid-State Electron. **24**, 981 (1981).
[54]S. M. Sze and K. K. Ng, *Physics of Semiconductor Devices*, 3rd ed. (Wiley, New Jersey, 2007).
[55]T. Hashizume, J. Kotani, A. Basile, and M. Kaneko, Jpn. J. Appl. Phys., Part 2 **45**, L111 (2006).